Global and Planetary Change 216 (2022) 103914

Contents lists available at ScienceDirect

Global and Planetary Change

journal homepage: www.elsevier.com/locate/gloplacha

Improving paleoenvironment in North China aided Triassic biotic recovery on land following the end-Permian mass extinction

Zhicai Zhu [a,b], Yongqing Liu [a,*], Hongwei Kuang [a,*], Andrew J. Newell [c,*], Nan Peng [a], Mingming Cui [a], Michael J. Benton [b,*]

[a] Institute of Geology, Chinese Academy of Geological Sciences, Beijing 100037, China
[b] School of Earth Sciences, University of Bristol, Bristol BS8 1RJ, UK
[c] British Geological Survey, Maclean Building, Wallingford OX10 8BB, UK

ARTICLE INFO

Editor: Maoyan Zhu

Keywords:
Triassic recovery
Ermaying Formation
Anisian
Lacustrine system
Sedimentary environment
Ordos Basin

ABSTRACT

The driver of the Early–Middle Triassic biotic recovery on land following the end-Permian crisis is puzzling. Here, we show the biotic recovery was gradual and spanned up to 8 Myr after the end-Permian mass extinction, based on continuous, well-dated sections over large areas in the northeastern Ordos Basin, North China. Initial recovery began in the Olenekian, marked by the disappearance of microbially induced sedimentary structures and reappearance of bioturbation, and continued in the Anisian, with a bloom of plants and tetrapods and intense bioturbation. Sedimentary environments changed from Induan braided-eolian conditions to Olenekian–Anisian shallow lacustrine and meandering river systems, marking an overall deepening lacustrine system. Carbonate $\delta^{13}C$ and geochemical proxies of weathering intensity, salinity and clayiness reveal an overall warm and semi-humid paleoclimate in the Olenekian–Anisian. This improved stable paleoenvironment of warm and semi-humid conditions likely contributed to the biotic recovery following the Permian-Triassic hyperthermal-related crisis.

1. Introduction

Around 252 Myr ago, the end-Permian mass extinction (EPME) wiped out over 81% of marine species and ~89% of continental species (Fan et al., 2020; Viglietti et al., 2021), making it the most severe extinction event in the Phanerozoic. The Earth underwent drastic environmental change and ecological collapse across the Permian-Triassic boundary (PTB) in the sea and on land (Algeo et al., 2011; Benton and Newell, 2014; Dal Corso et al., 2022). The PTB crisis was probably triggered by massive volcanic eruptions in Siberia (Burgess et al., 2017; Elkins-Tanton et al., 2020), which led to widespread acid rain, ocean acidification and mass wasting in which large volumes of sediment were washed from land into shallow seas (Newell et al., 1999; Sephton et al., 2005; Algeo and Twitchett, 2010), terrestrial aridity (Smith and Botha-Brink, 2014) and the input of greenhouse gases causing warming of land and oceans (Ward et al., 2000; Huey and Ward, 2005; Sun et al., 2012) as well as stagnation and ocean floor anoxia (Wignall and Twitchett, 1996; Isozaki, 1997; Payne et al., 2004). The delayed recovery of life through the Early–Middle Triassic (Chen and Benton, 2012; Zhao et al., 2020), however, is an unexpected aspect of the EPME crisis that has been explained by the prolonged environmental stress of repeated massive volcanism from the Siberian Traps causing flash warming and acid rain (e.g., Sun et al., 2012; Elkins-Tanton et al., 2020). The timing, processes, and causality for the crisis and recovery are all questioned and hotly debated (Benton and Twitchett, 2003; Chen and Benton, 2012; Grasby et al., 2019; Viglietti et al., 2021; Dal Corso et al., 2022).

Evidence of highly stressed ecosystems in the wake of the EPME has been noted in many marine and terrestrial sections. Marine systems suffered disruptions to oxygen cycling from surface to depths and many seabeds became anoxic (Payne et al., 2004), showing gaps in the sedimentary record (e.g., coral gap in the ocean and coal gap on land; Retallack et al., 1996; Schneebeli-Hermann, 2020; Zhao et al., 2020) and global warming (Knoll et al., 2007; Grasby et al., 2019; Wignall et al., 2019). Terrestrial environments underwent enhanced continental denudation and weathering (Algeo and Twitchett, 2010) and are

Abbreviations: EPME, end-Permian mass extinction; PTB, Permian-Triassic boundary; CIA, chemical index of alteration; CIW, chemical index of weathering; PIA, plagioclase index of alteration; ICV, index of compositional variability; MISS, microbially induced sedimentary structures.

* Corresponding authors.
E-mail addresses: liuyongqing@cags.ac.cn (Y. Liu), kuanghw@126.com (H. Kuang), ajn@bgs.ac.uk (A.J. Newell), mike.benton@bristol.ac.uk (M.J. Benton).

https://doi.org/10.1016/j.gloplacha.2022.103914
Received 28 February 2022; Received in revised form 27 July 2022; Accepted 3 August 2022
Available online 8 August 2022

distinguished by the coal gap, some 8–10 Myr when forest mires and wetlands were absent or markedly suppressed (Retallack et al., 1996; Schneebeli-Hermann, 2020), which attracts attention to the exact paleoenvironmental conditions. While environmental conditions in the Early Triassic are poorly understood, and the scale of the delayed recovery could be real or reflect some lack of sampling or fossilization (Brayard et al., 2009), it is important to explore sedimentary environmental evolution to understand the patterns and causes for the biotic recovery on land.

Here, we use integrated sedimentological, paleoecological, geochemical and geochronological analysis from four representative Early–Middle Triassic sections in the northeastern Ordos Basin, North China (Figs. 1 and 2, Tables DR1 and DR2) to show that improving paleoclimate in North China aided Triassic biotic recovery on land following the EPME. This study substantiates the environmental transition from Induan braided river-eolian conditions to Olenekian-Anisian shallow lacustrine and meandering river environments (Zhu et al., 2020).

2. Materials and methods

2.1. Section location

Terrestrial Permian-Triassic strata are widely distributed across the Ordos Basin in North China and comprise mainly alluvial deposits sourced from the Yin Mountain Belt. From Lopingian to Middle Triassic there is limited evidence for major tectonic activity or changes in sediment routing from mountain belt to adjacent foreland basin, increasing the likelihood that the stratigraphy was modulated primarily by major global climate change events associated with the EPME (Yang et al., 2017). Four sections were measured, in Fugu County (260 m-thick, 39°02′12.67″ N, 111°1′14.10″ E to 39°02′26.20″ N, 111°1′10.84″ E), Dongzhai Town (680 m-thick, 38°45′59.60″ N, 112°4′50.22″ E to 38°42′24.28″ N, 112°2′56.03″ E), Wupu County (360 m-thick, 37°38′45.27″ N, 110°47′52.92″ E to 37°52′35.03″ N, 110°46′48.22″ E) and Yushe County (140 m-thick, 37°06′10.69″ N, 112°53′26.72″ E to 37°05′29.21″ N, 112°53′9.11″ E) in the northeastern Ordos Basin, ca. 500–600 km west to southwest of Beijing (Figs. 1–3).

All sections are well exposed and preserve detailed sedimentary facies (also tuff of claystone) and abundant fossils such as microbially induced sedimentary structures (MISS), tetrapods and invertebrates that enable dating and provide evidence of the biotic recovery. Dating is constrained by biostratigraphy and U-Pb ages of zircons from interbedded tuff and detrital sandstone. Paleoclimate and weathering intensity were examined through soil carbonate $\delta^{13}C$, $\delta^{18}O$, and geochemical proxies, while the timing and potential drivers of biotic recovery were interpreted from sedimentary facies, zircon U-Pb geochronology and fossil evidence.

2.2. Zircon U-Pb dating

Bulk samples of tuffs and detrital sandstone were collected for zircon U-Pb dating to constrain the depositional age of the Heshanggou and Ermaying formations. Zircon grains were separated by conventional heavy-liquid and magnetic techniques at the Special Laboratory of the Geological Team of Hebei Province, Langfang, China. Cathodoluminescence (CL) and reflected and transmitted light images were obtained to investigate the origin and structure of zircons and to choose target sites for U-Pb analysis. CL images were obtained using a Hitachi S-3000 N scanning electron microscope fitted with a Gatan Chroma cathodoluminescence imaging system at the Institute of Geology, Chinese Academy of Geological Sciences (CAGS), Beijing, China.

Zircon U-Pb analyses of sample 20150625–2 were undertaken by SHRIMP II in the Beijing SHRIMP Center, Institute of Geology, Chinese Academy of Geological Sciences. The analytical procedures and conditions were similar to those described by Williams (1998). A primary O_2- ion beam was 2.5–3.5 nA and the spot size was ~25 μm. Standard zircons M257 (Nasdala et al., 2008) and TEMORA 1 (age = 417 Ma, Black et al., 2003) were used for calibration of elemental abundance and $^{206}Pb/^{238}U$ ratio, respectively. Data were generated by five scans. The standard to unknown ratio is 1:3 or 1:4. A common lead correction was based on the measured ^{204}Pb abundances and common Pb composition for the likely age of the rocks (Cumming and Tsong, 1975). Data processing was carried out using the Squid and Isoplot programs (Ludwig, 2003).

Zircon U-Pb analyses of the remaining five samples were undertaken by laser-ablation-inductively coupled plasma-mass spectrometry (LA-ICP-MS) at the Institute of Mineral Resources, CAGS, Beijing, China (samples 20160417–1, 20160416–2) and Beijing Creaech Testing Technology Co. Ltd. (samples DZHS062, DZEM103, and FGEM203), China. The detailed analytical process is given by Zhu et al. (2019). Laser sampling was performed using an ESI NWR 193 nm laser ablation system, and an AnlyitikJena PQMS Elite ICP-MS instrument was used to acquire ion-signal intensities. The analyses were carried out with a beam

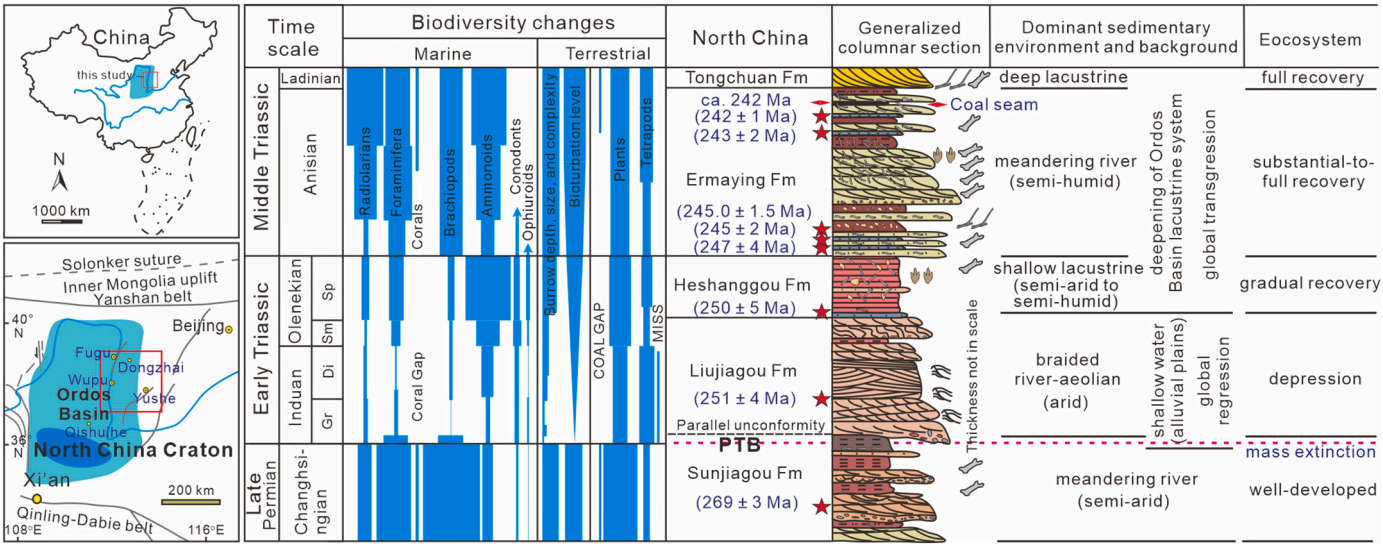

Fig. 1. Maps, global biodiversity variations, generalized columnar section, environmental changes and from the latest Permian to Middle Triassic in North China (modified after Chen and Benton, 2012; Zhu et al., 2020). Details see Fig. 2, Table DR1. Gr, Griesbachian; Di, Dienerian; Sm, Smithian; Sp, Spathian.

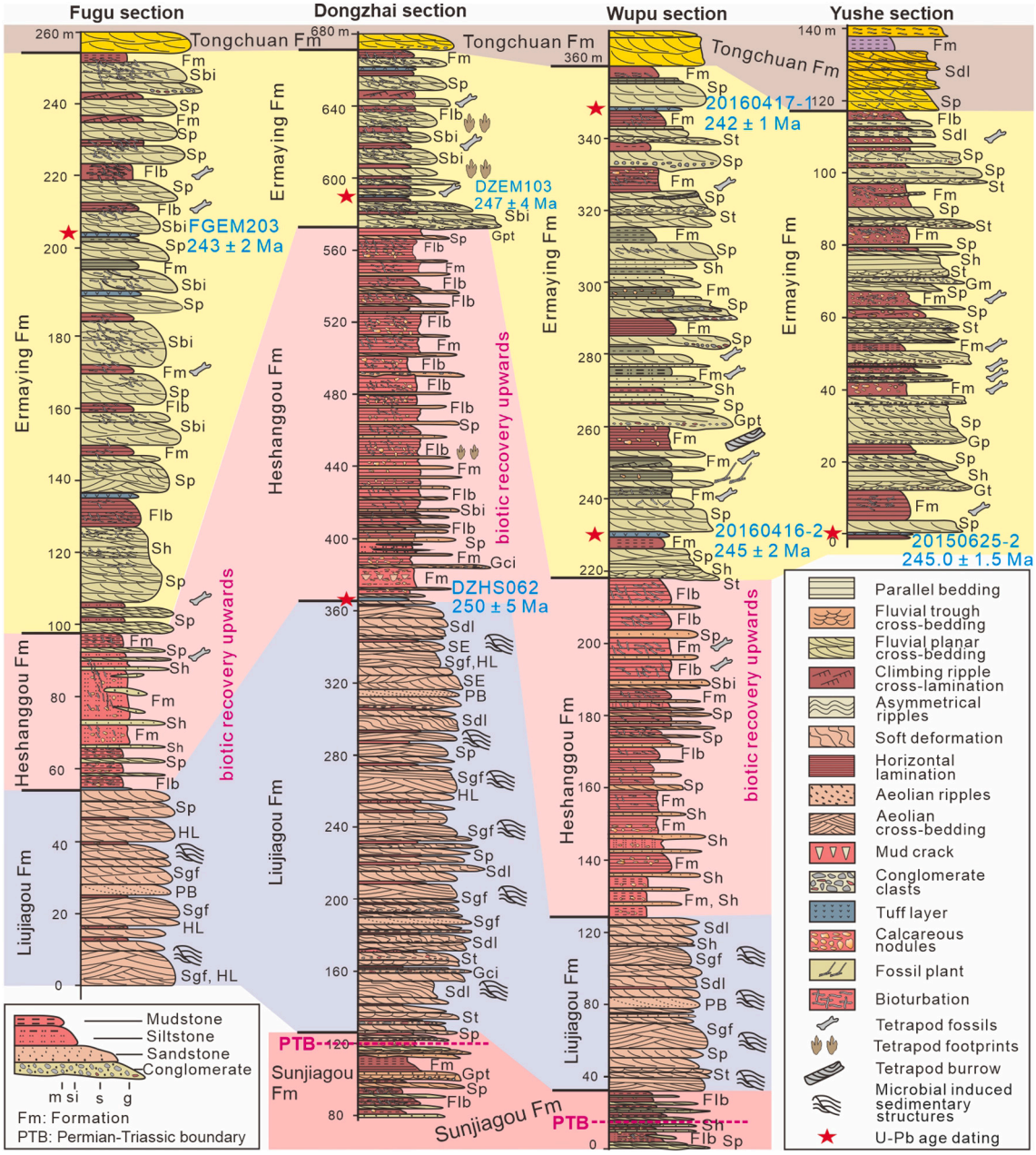

Fig. 2. Measured stratigraphic sections. Four locations across the Ordos Basin, North China, distinguishing major facies associations (details see Table DR2).

diameter of ~25 μm, a repetition rate of 10 Hz, and an energy of 4 J/cm^2. The analytical procedures followed those described by Hou et al. (2009). Off-line raw data selection and integration of background and analyte signals, and time-drift correction and quantitative calibration for U-Pb dating, were performed by ICP-MS-DataCal (Liu et al., 2009). The age calculations and Concordia and density diagrams were made using Isoplot/Ex ver 3.0 (Ludwig, 2003). During the analysis, the zircon standard GJ-1 and NIST SRM 610 were used as external standard for trace elements and U-Pb zircon dating separately and the Plešovice (337 ± 1 Ma) was dated as unknown samples, so as to evaluate accuracy and precision (Jackson et al., 2004; Sláma et al., 2008). We employ the time-resolved data acquisition to evaluate zircon homogeneity and to allow selective integration of signals to minimize common Pb contributions and Pb loss, and therefore to maximize concordance. Samples with concordance >90% are selected to generate the diagrams.

For tuff samples, the $^{207}Pb/^{206}Pb$ ages were used to assess the age. For the sandstone sample from the Heshanggou Formation (DZHS062), the $^{207}Pb/^{206}Pb$ ages were used to assess ages younger than 1000 Ma and $^{207}Pb/^{205}Pb$ ages were used to assess ages older than 1000 Ma. The weighted mean age of the youngest coherent U-Pb age cluster of the sandstone sample (this study, $n = 3$) was used to assess the maximum depositional age.

2.3. $\delta^{13}C$ and $\delta^{18}O$ analysis

Paleosol carbonate samples were selected from strata with clear indicators of soil development, including bioturbation, pedogenic structure, and lack of primary laminae and bedding. To avoid weathered surfaces and minimize the possible effects of diffusion and diagenesis (Cerling and Quade, 1993), each sample was collected at least ~50 cm below the section surface. The detailed analytical process is given by Zhu et al. (2019). All isotope ratios are given in ‰ relative to PDB. Carbon and oxygen isotopic results were used to estimate palaeotemperature (Cerling, 1984; Yapp and Poths, 1996), weathering

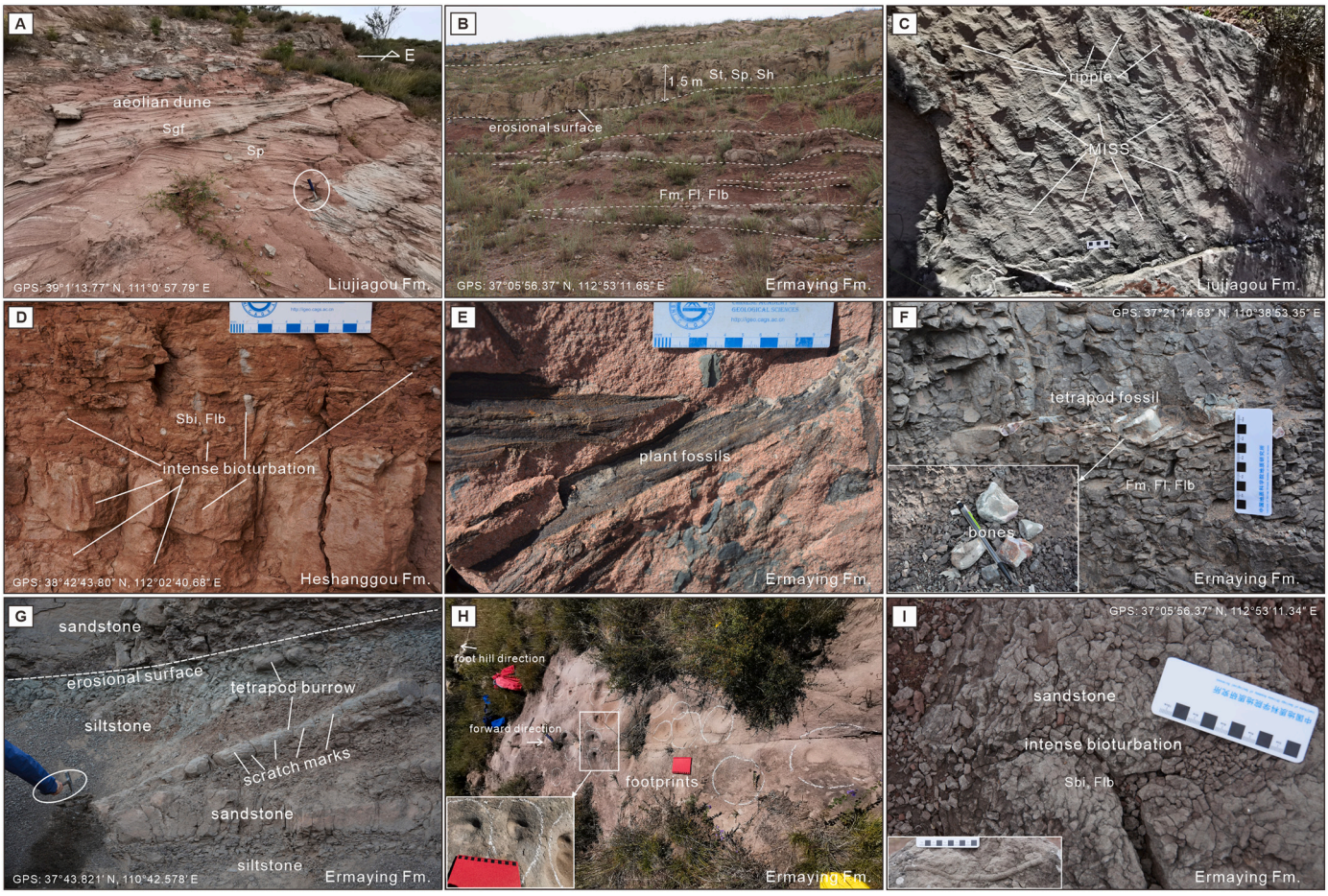

Fig. 3. Outcrop photos. (A) Variable cross bedding formed in braided-eolian deposits of the Liujiagou Formation. (B) Typical meandering sequences in the Ermaying Formation, where later accretion and erosional surfaces are common. (C) MISS preserved in the Liujiagou Formation with rare other biological evidence, representing the depressed paleoecology. They often coexist with ripples, deposited in a fluvial environment. (D) Ichnofossils preserved in greyish-green medium-grained sandstone interlayers of the Heshanggou Formation, deposited in a shallow-shore lake environment. (E) Plant (root) fossils from the Ermaying Formation, indicating the recovery of plants. (F-H) tetrapod bone fossils, burrows and footprints of tetrapods from the Ermaying Formation. A number of scattered bone fossils, burrows and footprints have been identified in multiple localities in eastern Ordos Basin, indicating the substantiate-full recovery of tetrapods. A huge number of tetrapods (e.g., huge herbivore Sinokannemeyeria) require abundant vegetation in a warm and semi-humid environment. (I) Intense bioturbation from the outcrop of the Ermaying Formation. Fm, Formation. (For interpretation of the references to colour in this figure legend, the reader is referred to the web version of this article.)

intensity (Passey et al., 2009) and atmospheric CO_2 (Yapp and Poths, 1996).

2.4. Geochemical analysis

Whole-rock major element compositions of mudstone samples were analyzed at the National Research Center for Geoanalysis, CAGS, Beijing. The detailed analytical process is given by Zhu et al. (2019). Calibration and correlation of calcium (CaO*, Nesbitt and Young, 1982), calculations of the chemical index of alteration (CIA, Nesbitt and Young, 1982), chemical index of weathering (CIW, Harnois, 1988), plagioclase index of alteration (PIA, Fedo et al., 1995) and index of compositional variability (ICV, Cox et al., 1995) are shown as follows, where each of the elemental concentrations is converted to moles:

$$CaO^{*} = min\,(CaO – 10/3 \times P_2O_5, Na_2O)$$

$$CIA = 100 \times Al_2O_3/(Al_2O_3 + K_2O + Na_2O + CaO^{*})$$

$$CIW = 100 \times Al_2O_3/(Al_2O_3 + Na_2O + CaO^{*})$$

$$PIA = 100 \times [(Al_2O_3 – K_2O)/(Al_2O_3 + Na_2O + CaO^{*} – K_2O)]$$

$$ICV = (Fe_2O_3 + K_2O + Na_2O + CaO^{*} + MgO + MnO + TiO_2)/(Al_2O_3)$$

2.5. Climate reconstruction

The reconstruction of climate in this study is based mainly on sedimentology, supported by paleontological and geochemical data. In the Early Triassic (Induan), evidence of eolian activity in the braided river deposits, and turbidite-like sand-sized loads in laminated couplets resulting from successive sheetwash events similar to examples in Karoo basin are important indicators of aridity (Smith and Botha-Brink, 2014; Zhu et al., 2020). We also considered coeval evidence of oscillatory hyper-warm and extreme hazards (e.g., hurricanes) from lacustrine deposits of the southern Ordos Basin (Ji et al., 2021), results of hyper-warm temperatures across the Paleo-Tethys Ocean based on oxygen isotope and climate model simulations (Sun et al., 2012; Penn et al., 2018), geochemical indices (e.g., reduced weathering intensity) and paleontological data (e.g., drought-tolerant plants, MISS) (Chu et al., 2015; Wignall et al., 2019; Zhu et al., 2020 and references therein) as evidence for unstable and stressed conditions. Similarly, fluvial transitions, climate-indicative biotic conditions (e.g., reappearance of peat-forming forests in wetlands) and geochemical proxies were combined to summarize climate changes in the Olenekian-Anisian.

3. Results

3.1. Stratigraphy and sedimentary facies

The Permian-Triassic successions in the Ordos Basin comprises the Sunjiagou (Lopingian), Liujiagou (Induan), Heshanggou (Olenekian), Ermaying (Anisian) and Tongchuan (Ladinian) formations, all deposited in continental fluvial-lacustrine environments (Figs. 1 and 2, Table DR2; Zhu et al., 2020).

The Liujiagou Formation is predominantly sandstone with occasional mudstone. Maroon intraformational mudrock clasts are common overlying irregular scour surfaces at the base of 1–5 m thick cross-bedded and horizontally laminated sandstone bodies. These associations represent channel fills and bars of braided river deposits. Fluvial deposits interbed with sandstones of eolian origin, which overlie sharp sand-drift surfaces and show lamination styles (inverse graded, pinstripe, grainflow and grainfall) that are typical of eolian ripples and dunes (Figs. 2 and 3A, Table DR2). The Liujiagou Formation was deposited on an arid alluvial plain in the northeastern part of the Ordos Basin, which probably passed basinwards into lacustrine-delta and lacustrine environments in the south (Ji et al., 2021).

The Heshanggou Formation is mainly horizontally laminated red mudstones and siltstones with some thin medium-grained sandstone beds, which may preserve mud cracks on their base. Beds of these fine-grained deposits have a tabular geometry and show high lateral continuity across outcrops. Coarse-grained sandstones and conglomerates are nearly absent and current-generated structures are rare. The Heshanggou Formation was deposited in a shallow lacustrine environment with some episodes of subaerial exposure (Fig. 2, Table DR2).

The Ermaying Formation is a fluvial succession of greenish-gray cross-bedded sandstones and subordinate dark red mudstone (Fig. 2; Fig. 3B). The sandstones are organized into fining-upward rhythmic units with pebbly sandstones resting on an erosional base passing upwards into trough cross-bedded, planar cross-bedded and parallel-laminated sandstone. These sandstone associations often terminate in dark red siltstones/mudstones with occasional calcareous nodules, and it is probable that they represent laterally accreted point bar deposits. The Ermaying Formation was probably deposited in meandering channel and floodplain environments under a relatively humid environment.

3.2. Geochronology

Five samples of interlayered tuffs from bottom to top of the Ermaying Formation (Fig. 2) give very similar mean $^{206}Pb/^{238}U$ ages of 247 ± 4 Ma, 245 ± 2 Ma, 245.0 ± 1.5 Ma, 243 ± 2 Ma, and 242 ± 1 Ma (Fig. 4A-E), and they generally young up-section but overlap within error, and may constrain the depositional age as Anisian. A sample of sandstone near the base of the Heshanggou Formation gives the youngest detrital zircon mean $^{206}Pb/^{238}U$ age of 250 ± 5 Ma (n = 3, Fig. 4F), which suggests its maximum depositional age might be Olenekian. These results are consistent with previous detrital zircon age constraints on the Lopingian Sunjiagou and Induan Liujiagou formations (Zhu et al., 2019), the Olenekian Heshanggou Formation (Nesbitt et al., 2010; Butler et al., 2019) and Anisian Ermaying Formation (Liu et al., 2018; Zhao et al., 2020; Jin et al., 2021).

3.3. Paleontological evidence

Abundant fossils (e.g., tetrapods, plants, bioturbation) from the Permian-Triassic strata in North China provide good constraints for the end-Permian crisis and the subsequent biotic recovery during the Early–Middle Triassic (Fig. 1, Table DR1, also see Zhu et al., 2020 and references therein). The PTB is identified about 20 m below the top of the Sunjiagou Formation by the earliest Triassic *Lundbladispora-Aratrisporites-Taeniaesporites* assemblage (Chu et al., 2015), further supported by the disappearance of bioturbation and tetrapod fossils, and a synchronous sharp negative shift of carbon isotopes and geochemical perturbation (Zhu et al., 2019). We note that evidence for life (e.g.,

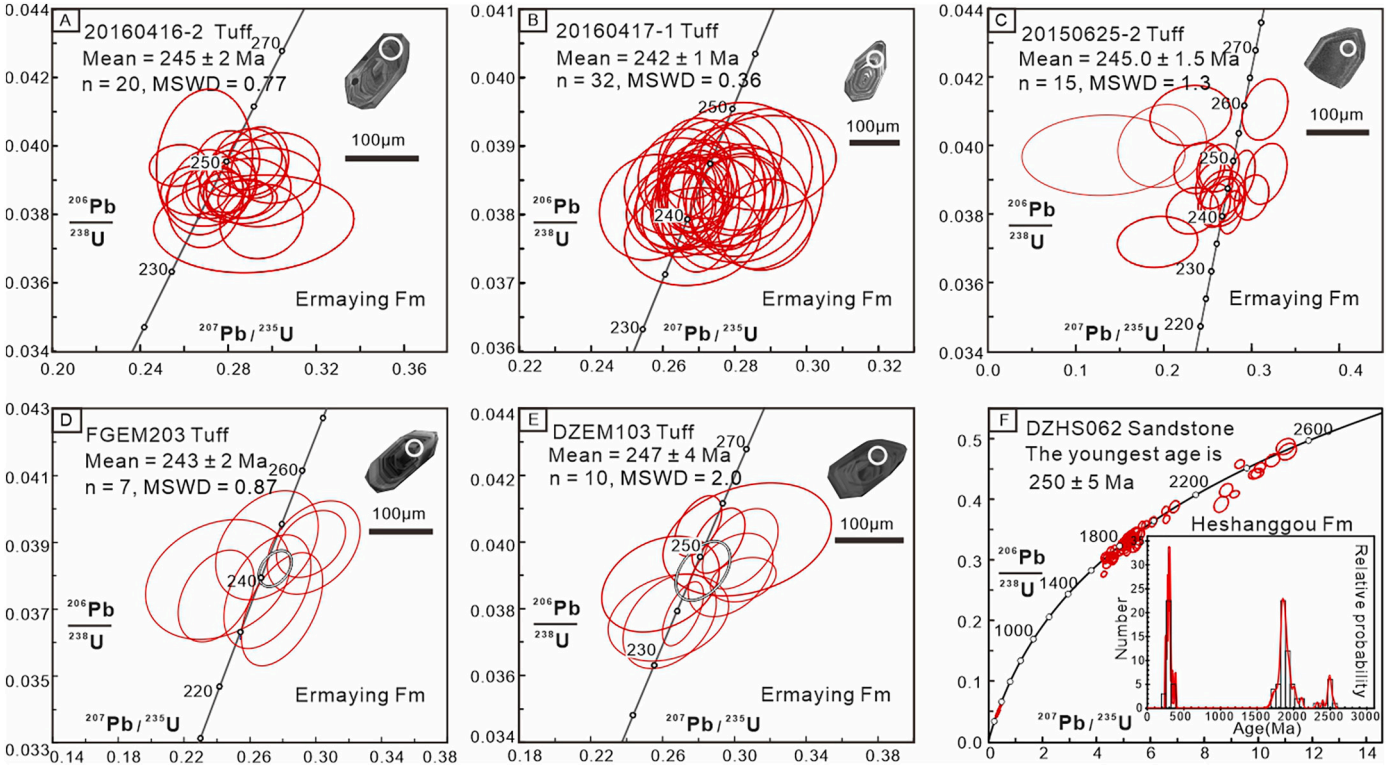

Fig. 4. Zircon U–Pb ages of tuff interlayers and sandstones. Analyses of five specimens (A–E) from the Ermaying Formation, and one (F) from the Heshanggou Formation (further details in Tables DR3 and DR4).

tetrapod fossils, bioturbation) disappeared near the top of the Sunjiagou Formation, consistent with the biotic crisis horizon. Abundant MISS but few other fossils occur in the Liujiagou Formation, indicating limited metazoan life (Fig. 3C). Tetrapods (including occasional footprints) and invertebrate trace fossils first occur at the base of the Heshanggou Formation and become more frequent and increasingly diverse upwards (Figs. 2 and 3D). Fossil diversity increases notably in the Ermaying Formation, including abundant plants, tetrapods (e.g., *Shansiodon* sp. nov.), tetrapod burrows, footprints and invertebrate trace fossils (Fig. 3E–I). Importantly, the first reappearance of coal seams was identified at the top of the Ermaying Formation from Qishuihe in the southern Ordos Basin (Zhao et al., 2020).

3.4. Geochemical evidence

The Mn/Sr ratio (mostly, 2.0–3.0), $\delta^{18}O$ and $\delta^{13}C$ cross-plot (Fig. DR1), and relatively stable Ti/Al ratio (0.05–0.08) throughout the Heshanggou and Ermaying formations suggest that samples were nearly unaltered, and data are reliable for paleoenvironmental reconstruction. The A-CN-K (Al_2O_3–CaO + Na_2O–K_2O) diagram (Fig. DR2) also suggests that they have undergone little diagenetic K metasomatism (Fedo et al., 1995; Perri, 2020). Values of the $\delta^{13}C$ and $\delta^{18}O$ profiles in the Heshanggou and Ermaying formations range consistently from −2.6‰ to −7.6‰ (VPDB) and −9.8‰ to −16.5‰ (VPDB) (Fig. 5). Geochemical proxies show moderate weathering intensity (56.24–75.75 of CIA, 67.85–92.57 of CIW, and 58.66–90.45 of PIA), low salinity change in fresh water (mostly 0.42–0.48 for [K + Na]/Al), little effect of deposition recycling (1.22–1.57 of ICV), and clayiness (Al/Si) and they are consistent with the overall semi-humid climatic conditions (Fig. 5).

4. Discussion

4.1. Biotic recovery after the EPME

Life began to recover quickly in the Early Triassic, but full recovery took some 8–9 Myr or longer in the sea and on land (Chen and Benton, 2012; Benton and Newell, 2014; Zhao et al., 2020). What prolonged the Early Triassic recovery and whether this delay was a result of complex ecosystem dynamics or stress of physical environmental conditions or a combination of both, remains enigmatic. In North China, our data show that the mass extinction events occurred near the top of the Sunjiagou Formation, revealed by the disappearance of bioturbation and tetrapod fossils, but ecosystems remained markedly suppressed above the PTB, shown by abundant MISS with other rare fossils in the Liujiagou

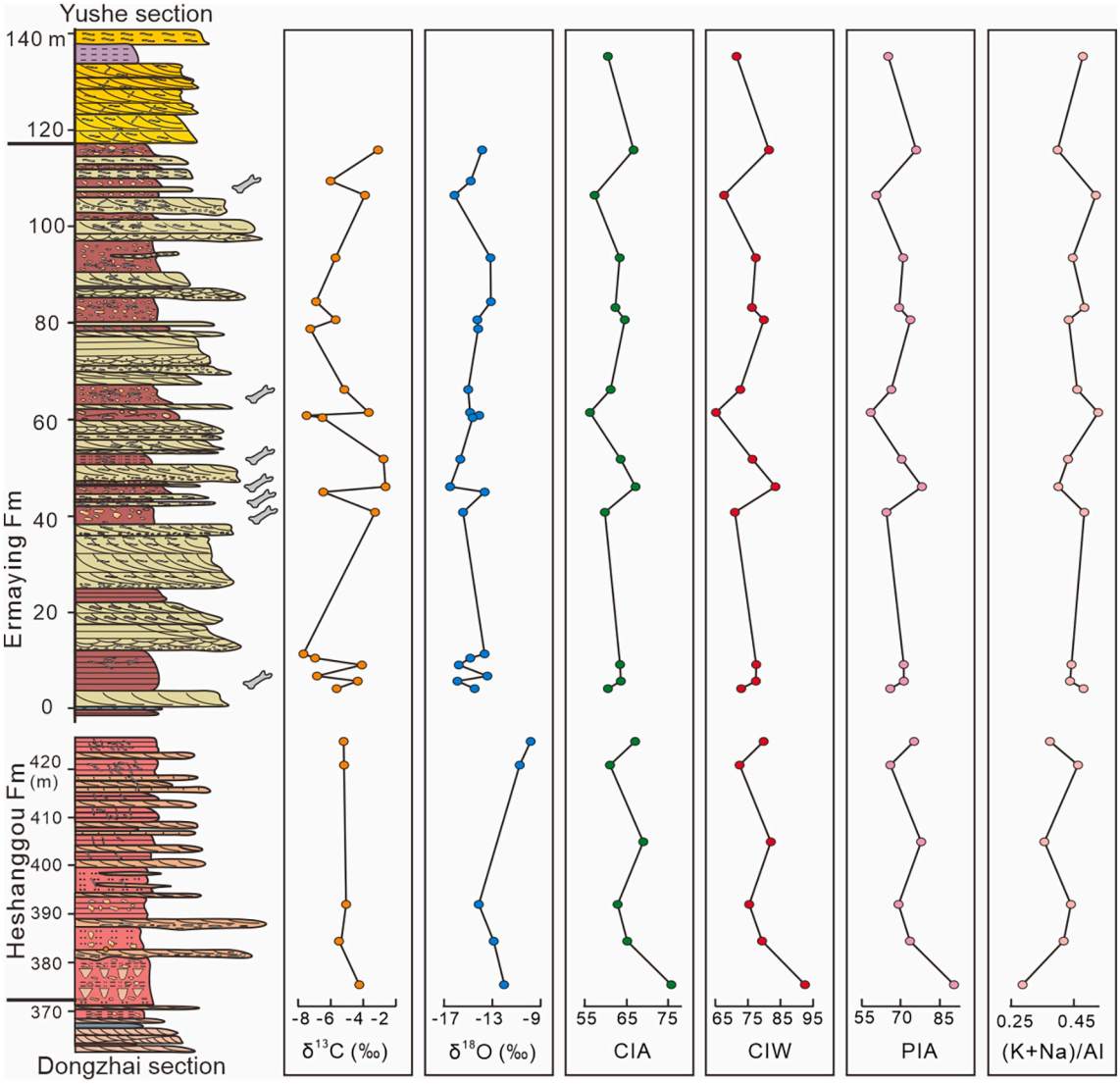

Fig. 5. $\delta^{13}C$, $\delta^{18}O$ and geochemical proxy profiles. Profiles through the Heshanggou and Ermaying formations (Fm) in the Yushe section, showing stable isotopes ($\delta^{13}C$, $\delta^{18}O$) from soil profiles, and the other metrics from mudstone (see Tables DR5 and DR6 for further details).

Formation (Fig. 3C). The Heshanggou Formation shows partial recovery, with increasing bioturbation upwards, as well as some plants and vertebrates (Fig. 3D). And then substantial-to-full recovery occurs in the Anisian Ermaying Formation [or so-called Yanchang Formation in some places (Jin et al., 2021)] at ca. 242 Ma, represented by intense bioturbation, blooms of tetrapods and plants and reappearance of coal seams (Fig. 3E–I; also see Zhao et al., 2020). This result is consistent with a fast recovery model of 1–3 Myr after the EPME (Song et al., 2011) and full recovery about 8–9 Myr after the EPME (Schneebeli-Hermann, 2020; Zhao et al., 2020).

4.2. Improving paleoenvironment during the Olenekian to Anisian

The reconstruction of climate in this study is based mainly on sedimentology, supported by paleontological and geochemical data. The evolution of sedimentary environments was driven largely by climate change, based on the absence of syndepositional tectonic activity in the North China Craton (Yang et al., 2017). River profiles became systematically straighter with increasing aridity because rivers flow infrequently and when they do, the discharge does not vary downstream (Chen et al., 2019). The transition from Lopingian meandering river systems to Induan braided streams was probably caused by increased erosion of uplands as forests were removed by acid rain coupled with increasing aridity and deteriorating paleoclimate during the PTB crisis (Benton and Newell, 2014; Smith and Botha-Brink, 2014; Zhu et al., 2020). We demonstrate that the depositional environments of the Liujiagou Formation provide evidence for low-frequency but high-magnitude precipitation under an overall arid paleoenvironment in the Induan. Some of the Liujiagou Formation in the southern Ordos Basin also experienced oscillatory extreme hazards of hurricanes connected to hyper-warm climate conditions across the Paleo-Tethys Ocean (Ji et al., 2021), consistent with previous results based on oxygen isotopes. Climate model simulations suggest that the hyper-warm temperatures were higher than 35 °C across the Paleo-Tethys Ocean adjacent to North China in the Early Triassic (Sun et al., 2012; Penn et al., 2018). Notably, the hyper warming and massive increases of atmospheric CO_2 emissions might have further amplified the unstable and extreme hydrological conditions (e.g., increasing aridity and abnormal weathering) and contributed to stressed conditions on land (Berg et al., 2016; Yang et al., 2022), which were the most typical characteristics during the earliest Triassic over wide areas (Ward et al., 2000; Smith and Botha-Brink, 2014; MacLeod et al., 2017; Fielding et al., 2019; Zhu et al., 2020; Ji et al., 2021; Ravidà et al., 2022; Dal Corso et al., 2022). The sedimentary transition in North China from Induan braided river and eolian conditions to Olenekian shallow lacustrine and Anisian meandering river systems, and its coincidence with an overall expansion of the deepening Ordos Basin lacustrine system in the Middle Triassic (Zhao et al., 2020; Jin et al., 2021), however, implies that the combination of pronounced humidity, increasing vegetation, recovery of soils and sea-level rise were the possible driving forces.

Fossil evidence supports the improved paleoclimate of overall warm and humid conditions (Table DR1). Widespread MISS in the Induan Liujiagou Formation document suppression of normal grazing activity by marine mollusks and other animals under harsh, oxygen-poor conditions (Wignall et al., 2019). However, MISS disappeared in the Heshanggou Formation with increasing bioturbation upwards, and increasingly abundant and varied plants and vertebrates. The recovery of these groups supports persistent and increasingly temperate-humid and an overall warm paleoenvironment in the Olenekian and Anisian, i.e., plants and tetrapods in the Heshanggou Formation suggest an overall semi-arid to semi-humid climate in lacustrine environments (Zhu et al., 2020 and references therein; Liu et al., 2022); coeval floras from Euramerica show an arid to wetland biome transition (Xiong et al., 2021). Burrows in the upper part of the Ermaying Formation in the Wupu section were probably formed by tetrapods such as the 100 kg herbivore *Sinokannemeyeria* (Fig. 3G, Yang et al., 2018), requiring abundant vegetation in a warm and semi-humid environment. Notably, improved paleoenvironmental conditions enabled the re-emergence of complex wetland paleoecosystems, which were probably the key to the restoration of complex peat-forming forests in the Anisian (~242 Ma), after the "coal-gap" hiatus of 10-Myr following the end-Permian crisis (Retallack et al., 1996, 2011; Zhao et al., 2020). The coincidence of an extraordinary diversification of freshwater ecosystems and expansion of the humid lacustrine system during the middle–late Triassic is supported by strong paleontological evidence (summarized in Table DR1; Zheng et al., 2018; Zhao et al., 2020).

Geochemically, carbonate $\delta^{13}C$ (−4.2‰–−5.2‰) and $\delta^{18}O$ (−9.8‰–−14.1‰) in the Heshanggou Formation suggest an overall semi-humid climate, but with several times of negative and positive shift in the Ermaying Formation ($\delta^{13}C$, −2.7‰–−7.6‰) and $\delta^{18}O$ (−13.2‰–−16.5‰), and their fluctuations are consistent with the weathering intensity changes revealed by CIA, CIW and PIA. These might indicate some seasonal precipitation in the early Anisian. The fluctuation of carbonate $\delta^{13}C$ in the Ermaying Formation may also reveal alternating intervals of methane storage and release connected with oscillating volcanism in the Anisian, or to occasional anoxic conditions with very large changes in organic burial rates. Further, carbon isotopes show similar positive and negative excursions from the later part of the Early Triassic to the Middle Triassic in marine sections of South China, further supporting possible similar forcing mechanisms of alternating intervals of methane storage and release or massive changes in the burial of organic and carbonate carbon under fluctuating oxic and anoxic conditions (Payne et al., 2004). The consistent negative shift of carbon isotopes and decreased weathering intensity (e.g., CIA and its modified version of ΔW) near the PTB interval and Induan Liujiagou Formation support an overall arid paleoclimate during the earliest Triassic (Zhu et al., 2019, 2020 and references therein), although the potential influence of organic matter sources and occasional precipitation still need to be further evaluated. Geochemical proxies of mudstones (e.g., overall moderate weathering intensity, stable salinity of freshwater) support overall moderate-to-highly weathered depositional conditions in the Heshanggou and Ermaying formations, with occasion fluctuations, and they show low-to-moderate levels and the existence of immature landscapes formed under a warm and semi-humid climate over wide areas in North China (Fig. 5).

4.3. Improving paleoenvironment aided the Triassic biotic recovery

Together, our evidence from sedimentology, paleontology and geochemistry agree on improving paleoenvironments across the huge continental Ordos Basin, allowing us to reconstruct Early–Middle Triassic paleoclimatic conditions on land and explore their connections with biotic recovery. Here, we show that the return of warm and humid paleoenvironments in the Olenekian and Anisian contributed to the biotic recovery in the Ordos Basin of North China (Guo et al., 2019; Yu et al., 2022), marking the end of the harsh and fluctuating paleoclimate in the Induan (e.g., arid, oscillatory hyper-warm and highly stressed conditions) that had delayed the recovery of stable ecosystems following the EPME (Benton, 2018; Grasby et al., 2019; Wignall et al., 2019; Hu et al., 2020; Liu et al., 2022; Zhu et al., 2020), An overall deepening and expanded Middle Triassic lacustrine system in the Ordos Basin linked with global sea-level rise may have triggered for the final steps of recovery (Zhao et al., 2020; Jin et al., 2021; Liu et al., 2021).

Even though the causes are debated, harsh environmental conditions can prolong biotic recovery (Wignall et al., 2019). There were several linked environmental challenges during the Early Triassic and earliest Middle Triassic, including periodic anoxia (Payne et al., 2004), global warming (Grasby et al., 2019), dry and cool conditions (Retallack et al., 2011), acidity (Borruel-Abadía et al., 2019), and highly unusual and stressed paleoenvironments (Wignall et al., 2019), and these factors are intertwined. On the other hand, our results over large areas in the northeastern Ordos Basin show that the development of livable

environmental (i.e., warm and semi-humid) conditions favor biotic recovery, and this process spanned up to 8 Myr. The link between improving paleoenvironments on land and global sea-level rise and implications for biotic recovery during the Middle Triassic is significant for better understanding of climate and livability across Pangea. Similar climatic changes (i.e., wet and dry) and biotic suppression and radiation have been noted elsewhere and are important issues for consideration of future global warming (Berg et al., 2016; Chen et al., 2019; Lindström et al., 2020; Trisos et al., 2020).

5. Conclusions

In this study, the reconstruction of climate based mainly on sedimentology, paleontological and geochemical data demonstrates that the improved paleoenvironment of warm and humid conditions during the Olenekian–Anisian likely contributed to the biotic recovery after the EPME. Sedimentary environments changed from Induan braided-eolian conditions to Olenekian–Anisian shallow lacustrine and meandering river systems, mainly influenced by increasing humidity in a relatively stable greenhouse world, accompanied by an overall expansion of deepening lacustrine systems in the Ordos Basin.

CRediT authorship contribution statement

Z.Z., Y.L., H.K. and M.J.B designed the project; Z.Z., Y.L., H.K., N.P. and M.C performed fieldwork and sampling; Z.Z. conducted the experiments and wrote the paper; Z.Z., Y.L., H.K., M.J.B., and A.J.N. revised the paper.

Declaration of Competing Interest

The authors declare that they have no known competing financial interests or personal relationships that could have appeared to influence the work reported in this paper.

Acknowledgments

This study was supported by the National Science Foundation of China (Grants 42288201, 41672111 and 41888101), the China Geological Survey Project (Grant DD20190005), the National Key Research and Development Program of China (Grant 2018YFC0604201), IGCP675, CAGS Research Fund (Grant S2004), the International Postdoctoral Exchange Fellowship Program (Grant 2020026), and NERC grant NE/P013724/1. We thank Shichao Xu, Liyang Dong, Peilin Xue and Gaowen Jia from the Shanxi Museum of Geology, Dr. Huan Xu from Yunnan University, Dr. Jun Liu and Jian Yi from IVPP, Chinese Academy of Sicences, as well as Wei An for their help in the field. Great help and insightful comments from the editor Dr. Maoyan Zhu, guest editor Dr. Tianchen He and two anonymous reviewers are greatly appreciated.

Appendix A. Supplementary data

Supplementary data to this article can be found online at https://doi.org/10.1016/j.gloplacha.2022.103914.

References

Algeo, T.J., Twitchett, R.J., 2010. Anomalous early Triassic sediment fluxes due to elevated weathering rates and their biological consequences. Geology 38, 1023–1026. https://doi.org/10.1130/G31203.1.

Algeo, T.J., Chen, Z.Q., Fraiser, M.L., Twitchett, R.J., 2011. Terrestrial–marine teleconnections in the collapse and rebuilding of early Triassic marine ecosystems. Palaeogeogr. Palaeoclimatol. Palaeoecol. 308, 1–11. https://doi.org/10.1016/j.palaeo.2011.01.011.

Benton, M.J., 2018. Hyperthermal-driven mass extinctions: killing models during the Permian-Triassic mass extinction. Phil. Trans. R. Soc. A 376, 0170076. https://doi.org/10.1098/rsta.2017.0076.

Benton, M.J., Newell, A.J., 2014. Impacts of global warming on Permo–Triassic terrestrial ecosystems. Gondwana Res. 25, 1308–1337. https://doi.org/10.1016/j.gr.2012.12.010.

Benton, M.J., Twitchett, R.J., 2003. How to kill (almost) all life: the end-Permian extinction event. Trends Ecol. Evol. 18, 358–365. https://doi.org/10.1016/S0169-5347(03)00093-4.

Berg, A., Findell, K., Lintner, B., Giannini, A., Seneviratne, S.I., van den Hurk, B., Lorenz, R., Pitman, A., Hagemann, S., Meier, A., Cheruy, F., Ducharne, A., Malyshev, S., Milly, P.C.D., 2016. Land–atmosphere feedbacks amplify aridity increase over land under global warming. Nat. Clim. Chang. 6, 869–874. https://doi.org/10.1038/nclimate3029.

Black, L.P., Kamo, S.L., Allen, C.M., Aleinikoff, J.N., Davis, D.W., Korsch, R.J., Foudoulis, C., 2003. TEMORA 1: A new zircon standard for Phanerozoic U–Pb geochronology. Chem. Geol. 200, 155–170. https://doi.org/10.1016/S0009-2541(03)00165-7.

Borruel-Abadía, V., Barrenechea, J.F., Galán-Abellán, A.B., De la Horra, R., López-Gómez, J., Ronchi, A., Luque, F.J., Alonso-Azcárate, J., Marzo, M., 2019. Could acidity be the reason behind the early Triassic biotic crisis on land?: Chem. Geol. 515, 77–86. https://doi.org/10.1016/j.chemgeo.2019.03.035.

Brayard, A., Escarguel, G., Bucher, H., Monnet, C., Bruhwiler, T., Goudemand, N., Galfetti, T., Guex, J., 2009. Good genes and good luck: Ammonoid diversity and the end-Permian mass extinction. Science 325, 1118–1121. https://doi.org/10.1126/science.1174638.

Burgess, S.D., Muirhead, J.D., Bowring, S.A., 2017. Initial pulse of Siberian Traps sills as the trigger of the end-Permian mass extinction. Nat. Commun. 8, 164. https://doi.org/10.1038/s41467-017-00083-9.

Butler, R., Ezcurra, M., Liu, J., Sookias, R., Sullivan, C., 2019. The anatomy and phylogenetic position of the erythrosuchid archosauriform *Guchengosuchus shiguaiensis* from the earliest Middle Triassic of China. PeerJ 7, e6435. https://doi.org/10.7717/peerj.6435.

Cerling, T.E., 1984. The stable isotopic composition of modern soil carbonate and its relationship to climate. Earth Planet. Sci. Lett. 71, 229–240. https://doi.org/10.1016/0012-821X(84)90089-X.

Cerling, T.E., Quade, J., 1993. Stable carbon and oxygen isotopes in soil carbonates. Geophysi. Monogr. 78, 217–231. https://doi.org/10.1029/GM078p0217.

Chen, Z.Q., Benton, M.J., 2012. The timing and pattern of biotic recovery following the end-Permian mass extinction. Nat. Geosci. 5, 375–383. https://doi.org/10.1038/NGEO1475.

Chen, S.A., Michaelides, K., Grieve, S.W.D., Singer, M.B., 2019. Aridity is expressed in river topography globally. Nature 573, 573–577. https://doi.org/10.1038/s41586-019-1558-8.

Chu, D., Tong, J., Song, H., Benton, M.J., Bottjer, D.J., Song, H., Tian, L., 2015. Early Triassic wrinkle structures on land: stressed environments and oases for life. Sci. Rep. 5 https://doi.org/10.1038/srep10109.

Cox, R., Lowe, D.R., Cullers, R.L., 1995. The influence of sediment recycling and basement composition on evolution of mudrock chemistry in the southwestern United States. Geochim. Cosmochim. Acta 59, 2919–2940. https://doi.org/10.1016/0016-7037(95)00185-9.

Cumming, G.L., Tsong, F., 1975. Variations in the isotopic composition of volatilized lead and the age of the western Granodiorite, Yellowknife, northwest Territories. Can. J. Earth Sci. 12, 558–573. https://doi.org/10.1139/e75-050.

Dal Corso, J., Song, H., Callegaro, S., Chu, D., Sun, Y., Hilton, J., Grasby, S., Joachimski, M., Wignall, P.B., 2022. Environmental crises at the Permian–Triassic mass extinction. Nat. Rev. Earth Environ. 1–18 https://doi.org/10.1038/s43017-021-00259-4.

Elkins-Tanton, L.T., Grasby, S.E., Black, B.A., Veselovskiy, R.V., Ardakani, O.H., Goodarzi, F., 2020. Field evidence for coal combustion links the 252 Ma Siberian Traps with global carbon disruption. Geology 48, 986–991. https://doi.org/10.1130/G47365.1.

Fan, J.X., Shen, S., Erwin, D., Sadler, P., MacLeod, N., Cheng, Q.-m, Hou, X.-d, Yang, J., Wang, X.-d, Wang, Y., Zhang, H., Chen, X., Li, G.X, Zhang, Y., Shi, Y.-K, Yuan, D., Chen, Q., Zhang, L.N, Li, C., Zhao, Y.Y., 2020. A high-resolution summary of Cambrian to early Triassic marine invertebrate biodiversity. Science 272–277. https://www.science.org/doi/10.1126/science.aax4953.

Fedo, C.M., Wayne Nesbitt, H., Young, G.M., 1995. Unraveling the effects of potassium metasomatism in sedimentary rocks and paleosols, with implications for paleoweathering conditions and provenance. Geology 23, 921–924. https://doi.org/10.1130/0091-7613(1995)023<0921:UTEOPM>2.3.CO;2.

Fielding, C.R., Frank, T.D., McLoughlin, S., Vajda, V., Mays, C., Tevyaw, A.P., Winguth, A., Winguth, C., Nicoll, R.S., Bocking, M., Crowley, J.L., 2019. Age and pattern of the southern high-latitude continental end-Permian extinction constrained by multiproxy analysis. Nat. Commun. 10, 385. https://www.nature.com/articles/s41467-018-07934-z.

Grasby, S.E., Knies, J., Beauchamp, B., Bond, D.P.G., Wignall, P., Sun, Y.D., 2019. Global warming leads to early Triassic nutrient stress across northern Pangea. Geol. Soc. Am. Bull. 132, 943–954. https://doi.org/10.1130/B32036.1.

Guo, W., Tong, J., Tian, L., Chu, D., Bottjer, D.J., Shu, W., Ji, K., 2019. Secular variations of ichnofossils from the terrestrial Late Permian–Middle Triassic succession at the Shichuanhe section in Shaanxi Province. North China. Glob. Planet. Change 181, 102978. https://doi.org/10.1016/j.gloplacha.2019.102978.

Harnois, L., 1988. The CIW index: a new chemical index of weathering. Sediment. Geol. 55, 319–322. https://doi.org/10.1016/0037-0738(88)90137-6.

Hou, K.J., Tian, Y.R., Li, Y.H., 2009. In situ U–Pb zircon dating using laser ablation-multi ion counting-ICP-MS [in Chinese with English Abstract]. Mineral Deposits 28, 481–492.

Hu, X., Li, J., Han, Z., Li, Y., 2020. Two types of hyperthermal events in the Mesozoic-Cenozoic: Environmental impacts, biotic effects, and driving mechanisms. Sci. China Earth Sci. 63, 1–18. https://doi.org/10.1007/s11430-019-9604-4.

Huey, R.B., Ward, P.D., 2005. Hypoxia, global warming, and terrestrial late Permian extinctions. Science 308, 398–401. https://doi.org/10.1126/science.1108019.

Isozaki, Y., 1997. Permo-Triassic boundary superanoxia and stratified superocean: Records from lost deep sea. Science 276, 235–238. https://doi.org/10.1126/science.276.5310.235.

Jackson, S.E., Pearson, N.J., Griffin, W.L., Belousova, E.A., 2004. The application of laser ablation-inductively coupled plasma-mass spectrometry to in situ U–Pb zircon geochronology. Chem. Geol. 211, 47–69. https://doi.org/10.1016/j.chemgeo.2004.06.017.

Ji, K.X., Wignall, P.B., Peakall, J., Tong, J.N., Chu, D.L., Pruss, S.B., 2021. Unusual intraclast conglomerates in a stormy, hot-house lake: the early Triassic North China Basin. Sedimentology 68, 3385–3404. https://doi.org/10.1111/sed.12903.

Jin, X., Baranyi, V., Caggiati, M., Franceschi, M., Wall, C.J., Liu, G., Schmitz, M.D., Gianolla, P., Ogg, J.G., Lu, G., Shi, Z., Preto, N., 2021. Middle Triassic lake deepening in the Ordos Basin of North China linked with global sea-level rise. Glob. Planet. Change 207, 103670. https://doi.org/10.1016/j.gloplacha.2021.103670.

Knoll, A.H., Bambach, R.K., Payne, J.L., Pruss, S., Fischer, W.W., 2007. Paleophysiology and end-Permian mass extinction. Earth Planet. Sci. Lett. 256, 295–313. https://doi.org/10.1016/j.epsl.2007.02.018.

Lindström, S., Bjerager, M., Alsen, P., Sanei, H., Bojesen-Koefoed, J., 2020. The Smithian–Spathian boundary in North Greenland: implications for extreme global climate changes. Geol. Mag. 157, 1547–1567. https://doi.org/10.1017/S0016756819000669.

Liu, Y., Gao, S., Hu, Z., Gao, C., Zong, K., Wang, D., 2009. Continental and oceanic crust recycling-induced melt-peridotite interactions in the trans-North China orogen: U–Pb dating, Hf Isotopes and trace elements in zircons from mantle xenoliths. J. Petrol. 51, 537–571. https://doi.org/10.1093/petrology/egp082.

Liu, J., Ramezani, J., Li, L., Shang, Q., Xu, G., Wang, Y., Yang, J., 2018. High-precision temporal calibration of Middle Triassic vertebrate biostratigraphy: U–Pb zircon constraints for the *Sinokannemeyeria* fauna and *Yonghesuchus*. Vertebrata PalAsiatica 55, 1–9. https://doi.org/10.19615/j.cnki.1000-3118.170808.

Liu, H., Qiu, Z., Zou, C., Fu, J., Zhang, W., Tao, H., Li, S., Zhou, S., Wang, L., Chen, Z.Q., 2021. Environmental changes in the Middle Triassic lacustrine basin (Ordos, North China): Implication for biotic recovery of freshwater ecosystem following the Permian-Triassic mass extinction. Glob. Planet. Change 204, 103559. https://doi.org/10.1016/j.gloplacha.2021.103559.

Liu, J., Abdala, F., Angielczyk, K.D., Sidor, C.A., 2022. Tetrapod turnover during the Permo-Triassic transition explained by temperature change. Earth-Sci. Rev. 224, 103886 https://doi.org/10.1016/j.earscirev.2021.103886.

Ludwig, K.R., 2003. User's manual for a geochronological toolkit for Microsoft Excel (Isoplot/Ex version 3.0). Berkeley Geochron. Center Spe. Pub. 4, 1–70.

MacLeod, K.G., Quinton, P.C., Bassett, D.J., 2017. Warming and increased aridity during the earliest Triassic in the Karoo Basin, South Africa. Geology 45, 483–486. https://doi.org/10.1130/G38957.1.

Nasdala, L., et al., 2008. Zircon M257 - a homogeneous natural reference material for the ion microprobe U–Pb analysis of zircon. Geostandards Geoanalytic. Res. 32, 247–265. https://doi.org/10.1111/j.1751-908X.2008.00914.x.

Nesbitt, H.W., Young, G.M., 1982. Early Proterozoic climates and plate motions inferred from major element chemistry of lutites. Nature 299, 715–717. https://doi.org/10.1038/299715a0.

Nesbitt, S.J., Liu, J., Li, C., 2010. A sail-backed suchian from the Heshanggou Formation (early Triassic: Olenekian) of China. Earth Environment. Sci. Trans. R. Soc. Edinburgh 101, 271–284. https://doi.org/10.1017/S1755691011020044.

Newell, A.J., Tverdokhlebov, V.P., Benton, M.J., 1999. Interplay of tectonics and climate on a transverse fluvial system, Upper Permian, Southern Uralian Foreland Basin, Russia. Sediment. Geol. 127, 11–29. https://doi.org/10.1016/S0037-0738(99)00009-3.

Passey, B.H., Ayliffe, L.K., Kaakinen, A., Zhang, Z., Eronen, J.T., Zhu, Y., Zhou, L., Cerling, T.E., Fortelius, M., 2009. Strengthened East Asian summer monsoons during a period of high-latitude warmth? Isotopic evidence from Mio-Pliocene fossil mammals and soil carbonates from northern China. Earth Planet. Sci. Lett. 277, 443–452. https://doi.org/10.1016/j.epsl.2008.11.008.

Payne, J.L., Lehrmann, D.J., Wei, J., Orchard, M.J., Schrag, D.P., Knoll, A.H., 2004. Large perturbations of the carbon cycle during recovery from the end-Permian extinction. Science 305, 506–509. https://doi.org/10.1126/science.1097023.

Penn, J.L., Deutsch, C., Payne, J.L., Sperling, E.A., 2018. Temperature-dependent hypoxia explains biogeography and severity of end-Permian marine mass extinction. Science 362 (6419), 1–6. https://doi.org/10.1126/science.aat1327.

Perri, F., 2020. Chemical weathering of crystalline rocks in contrasting climatic conditions using geochemical proxies: An overview. Palaeogeogr. Palaeoclimatol. Palaeoecol. 556, 109873 https://doi.org/10.1016/j.palaeo.2020.109873.

Ravidà, D.C.G., Caracciolo, L., Henares, S., Janßen, M., Stollhofen, H., Valdez, V., 2022. Drainage and environmental evolution across the Permo–Triassic boundary in the south-east Germanic Basin (north-east Bavaria). Sedimentology. 69, 501–536. https://doi.org/10.1111/sed.12913.

Retallack, G.J., Veevers, J.J., Morante, R., 1996. Global coal gap between Permian–Triassic extinction and Middle Triassic recovery of peat-forming plants. Geol. Soc. Am. Bull. 108, 195–207. https://doi.org/10.1130/0016-7606.

Retallack, G.J., Sheldon, N.D., Carr, P.F., Fanning, M., Thompson, C.A., Williams, M.L., Jones, B.G., Hutton, A., 2011. Multiple early Triassic greenhouse crises impeded recovery from late Permian mass extinction. Palaeogeogr. Palaeoclimatol. Palaeoecol. 308, 233–251. https://doi.org/10.1016/j.palaeo.2010.09.022.

Schneebeli-Hermann, E., 2020. Regime shifts in an early Triassic subtropical ecosystem. Front. Earth Sci. 8, 588696 https://doi.org/10.3389/feart.2020.588696.

Sephton, M.A., Looy, C.V., Brinkhuis, H., Wignall, P.B., de Leeuw, J.W., Visscher, H., 2005. Catastrophic soil erosion during the end-Permian biotic crisis. Geology 33, 941–944. https://doi.org/10.1130/G21784.1.

Sláma, J., Kosler, J., Condon, D.J., Crowley, J.L., Gerdes, A., Hanchar, J.M., Horstwood, M.S.A., Morris, G.A., Nasdala, L., Norberg, N., Schaltegger, U., Schoene, B., Tubrett, M.N., Whitehouse, M.J., 2008. Plešovice zircon-A new natural reference material for U–Pb and Hf isotopic microanalysis. Chem. Geol. 249, 1–35. https://doi.org/10.1016/j.chemgeo.2007.11.005.

Smith, R.M.H., Botha-Brink, J., 2014. Anatomy of a mass extinction: Sedimentological and taphonomic evidence for drought-induced die-offs at the Permo-Triassic boundary in the main Karoo Basin, South Africa. Palaeogeogr. Palaeoclimatol. Palaeoecol. 396, 99–118. https://doi.org/10.1016/j.palaeo.2014.01.002.

Song, H., Wignall, P.B., Chen, Z.Q., Tong, J.N., Bond, D.P.G., Lai, X.L., Zhao, X.M., Jiang, H.S., Yan, C.B., Niu, Z.J., Chen, J., Yang, H., Wang, Y.B., 2011. Recovery tempo and pattern of marine ecosystems after the end-Permian mass extinction. Geology 39, 739–742. https://doi.org/10.1130/G32191.1.

Sun, Y.D., Joachimski, M.M., Wignall, P.B., Yan, C.B., Chen, Y.L., Jiang, H.S., Wang, L.N., Lai, X.L., 2012. Lethally hot temperatures during the early Triassic greenhouse. Science 338, 366–370. https://www.science.org/doi/10.1126/science.1224126.

Trisos, C.H., Merow, C., Pigot, A.L., 2020. The projected timing of abrupt ecological disruption from climate change. Nature 580, 496–501. https://doi.org/10.1038/s41586-020-2189-9.

Viglietti, P.A., Benson, R.B.J., Smith, R.M.H., Botha, J., Kammerer, C.F., Skosan, Z., Butler, E., Crean, A., Eloff, B., Kaal, S., Mohoi, J., Molehe, W., Mtalana, N., Mtungata, S., Ntheri, N., Ntsala, T., Nyaphuli, J., October, P., Skinner, G., Strong, M., Stummer, H., Wolvaardt, F.P., Angielczyk, K.D., 2021. Evidence from South Africa for a protracted end-Permian extinction on land. Proc. Natl. Acad. Sci. U. S. A. 118, e2017045118 https://doi.org/10.1073/pnas.2017045118.

Ward, D., Montgomery, D.R., Smith, R., 2000. Altered river morphology in South Africa related to the Permian–Triassic extinction. Science 289, 1740–1743. https://doi.org/10.1126/science.289.5485.1740.

Wignall, P.B., Twitchett, R.J., 1996. Oceanic anoxia and the end Permian mass extinction. Science 272, 1155–1158. https://doi.org/10.1126/science.272.5265.1155.

Wignall, P.B., Bond, D.P.G., Grasby, S.E., Pruss, S.B., Peakall, J., 2019. Controls on the formation of microbially induced sedimentary structures and biotic recovery in the lower Triassic of Arctic Canada. Geol. Soc. Am. Bull. 132, 918–930. https://doi.org/10.1130/B35229.1.

Williams, J.S., 1998. U-Th-Pb geochronology by ion microprobe. Application of microanalytical techniques to understanding mineralizing processes. Geology 7, 1–35.

Xiong, C., Wang, J., Huang, P., Cascales-Miñana, B., Cleal, C.J., Benton, M.J., Xue, J., 2021. Plant resilience and extinctions through the Permian to Middle Triassic on the North China Block: a multilevel diversity analysis of macrofossil records. Earth-Sci. Rev. 223, 103846 https://doi.org/10.1016/j.earscirev.2021.103846.

Yang, D.B., Yang, H.T., Shi, J.P., Xu, W.L., Wang, F., 2017. Sedimentary response to the paleogeographic and tectonic evolution of the southern North China Craton during the late Paleozoic and Mesozoic. Gondwana Res. 49, 278–295. https://doi.org/10.1016/j.gr.2017.06.009.

Yang, J.S., Yi, J., Dong, L.Y., Yang, L.J., 2018. Tetrapod burrows from the Triassic Ermaying Formation of Shanxi, China. Vertebrate Palasiatica 56, 147–156. https://doi.org/10.19615/j.cnki.1000-3118.180319.

Yang, J.H., Cawood, P.A., Condon, D.J., Liu, J., Deng, X., Wang, J., Du, Y., Yuan, D., 2022. Anomalous weathering trends indicate accelerated erosion of tropical basaltic landscapes during the Permo-Triassic warming. Earth Planet. Sci. Lett. 577, 117256 https://doi.org/10.1016/j.epsl.2021.117256.

Yapp, C.J., Poths, H., 1996. Carbon isotopes in continental weathering environments and variations in ancient atmospheric CO_2 pressure. Earth Planet. Sci. Lett. 137, 71–82. https://doi.org/10.1016/0012-821X(95)00213-V.

Yu, Y., Tian, L., Chu, D., Song, H., Guo, W., Tong, J., 2022. Latest Permian–Early Triassic paleoclimatic reconstruction by sedimentary and isotopic analyses of paleosols from the Shichuanhe section in central North China Basin. Palaeogeogr. Palaeoclimatol. Palaeoecol. 585, 110726 https://doi.org/10.1016/j.palaeo.2021.110726.

Zhao, X.D., Zheng, D.R., Xie, G.W., Jenkyns, H.C., Guan, C.G., Fang, Y.A., He, J., Yuan, X.Q., Xue, N.H., Wang, H., Li, S., Jarzembowski, E.A., Zhang, H.C., Wang, B., 2020. Recovery of lacustrine ecosystems after the end-Permian mass extinction. Geology 48, 609–613. https://doi.org/10.1130/G47502.1.

Zheng, D., Chang, S.C., Wang, H., Fang, Y., Wang, J., Feng, C., Xie, G., Jarzembowski, E. A., Zhang, H., Wang, B., 2018. Middle-late Triassic insect radiation revealed by diverse fossils and isotopic ages from China. Sci. Adv. 4, eaat1380. https://doi.org/10.1126/sciadv.aat1380.

Zhu, Z., Liu, Y., Kuang, H., Benton, M.J., Newell, A.J., Xu, H., An, W., Ji, S., Xu, S., Peng, N., Zhai, Q., 2019. Altered fluvial patterns in North China indicate rapid climate change linked to the Permian-Triassic mass extinction. Sci. Rep. 9, 16818. https://doi.org/10.1038/s41598-019-53321-z.

Zhu, Z.C., Kuang, H.W., Liu, Y.Q., Benton, M.J., Newell, J., Xu, H., An, W., Ji, S.A., Xu, S. C., Peng, N., Zhai, Q.G., 2020. Intensifying aeolian activity following the end Permian mass extinction. evidence from the Late Permian–Early Triassic terrestrial sedimentary record of the Ordos Basin, North China. Sedimentology 67, 2691–2720. https://doi.org/10.1111/sed.12716.